GEOPHYSICS, VOL. 81, NO. 2 (MARCH-APRIL 2016); P. M1–M6, 4 FIGS., 1 TABLE.
10.1190/GEO2015-0194.1

Effect of thermal maturity on elastic properties of kerogen

Saeed Zargari[1], Taylor M. Wilkinson[2], Corinne E. Packard[2], and Manika Prasad[1]

ABSTRACT

We have performed spatially continuous nanodynamic mechanical analysis on four organic-rich shale samples with different thermal maturities to extract the elastic modulus of the kerogen particles. Aliquots were rigorously prepared, and three scans were acquired from each aliquot. Subcritical nitrogen adsorption pore characterization was performed to determine the abundance of kerogen-hosted porosity. To fully characterize the pore system of samples from the oil window, toluene and then chloroform extraction were performed to remove the pore-filling hydrocarbons prior to nitrogen adsorption. The statistical distribution of the measured modulus values was analyzed to extract the properties of the shale particles. In mature samples from the peak oil generation or gas window, the kerogen porosity was the dominant pore morphology. We found that significant lowering of the kerogen particle modulus resulted from intraparticle kerogen porosity. The kerogen particle modulus in mature samples was measured as being lower (7–12 GPa) than the immature sample (15–20 GPa) due to gas- or bitumen-filled pores.

INTRODUCTION

In self-sourcing reservoirs, maturity (extent of oil generation), porosity, and the abundance of natural fractures are the main parameters that make these tight plays economical. Determining sweet spots using spatially extensive detecting techniques is essential for successful development of these resources. Understanding the elastic behavior of source rocks and their interrelation with organic content and maturity can provide crucial information about the amount of generated hydrocarbon, petrophysical properties, and geomechanical characteristics from well logs and seismic surveys.

Generating representative rock models to describe the behavior of organic-rich rocks is challenging due to complex textural properties of these rocks and the uncertainties in the mechanical properties of some of the major components. Despite previous studies on the texture of organic-rich rocks in relation to their elastic properties, anisotropy (Vernik and Nur, 1992), and mechanical characteristics of the grains (Prasad, 2001; Zeszotarski et al., 2004; Ahmadov et al., 2009; Mba and Prasad, 2010; Prasad et al., 2011; Wilkinson et al., 2014; Eliyahu et al., 2015), there is limited available data on the characteristics of some essential components, such as clays and organic matter. Moreover, changes in the properties of kerogen and clay minerals during the course of thermal maturation are poorly understood.

Nanoindentation has been widely used for measuring the mechanical properties of thin films, fine-grained composites, and polycrystalline materials. The technique uses a diamond indenter to apply small-scale forces to a material while measuring the resulting displacement. Recently, this technique has gained tremendous attention for the characterization of geomaterials, especially fine-grained mudrocks (Prasad, 2001; Zeszotarski et al., 2004; Ulm and Abousleiman, 2006; Bobko and Ulm, 2008; Ahmadov et al., 2009; Kumar et al., 2012; Shukla, 2013; Zargari et al., 2013). The accuracy of measurements using this technique is limited by the sharpness of the tip, the size of the grains (in granular materials), or the thickness of the films (in thin films) in the substrate.

The effects of underlying and surrounding grains on nanoindentation measurements in very fine grain materials such as mudrocks can be significant. If the generated stress field exceeds the grain boundaries, measurements are affected by comingled properties of loaded grain(s) and the substrate and surrounding material (Constantinides et al., 2006; Ulm et al., 2010).

To avoid potential errors associated with the indentation size and depth of investigation, high-resolution, spatially continuous, dynamic mechanical probing techniques have been used (Prasad et al., 2002; Wilkinson et al., 2014; Eliyahu et al., 2015).

In this study, we implemented the nano-DMA technique. This technique provides a high-resolution 2D continuous measure of

Manuscript received by the Editor 21 March 2015; revised manuscript received 3 August 2015; published online 26 February 2016.
[1]Colorado School of Mines, Department of Petroleum Engineering, Golden, Colorado, USA. E-mail: szargari@mines.edu; mprasad@mines.edu.
[2]Colorado School of Mines, Department of Metallurgical and Materials Engineering, Golden, Colorado, USA. E-mail: twilkins@mines.edu; cpackard@mines.edu.

mechanical properties. For a complete description of the technique and the sample preparation requirements in organic-rich shales, we refer readers to Wilkinson et al. (2014). Because the presence of kerogen-hosted porosity affects the modulus of kerogen particles, separate aliquots underwent solvent extraction followed by nitrogen adsorption pore characterization to determine the abundance of intraparticle kerogen porosity. Pore morphology characteristics were further integrated with nano-DMA results to explain the mechanical behavior of kerogen particles.

MATERIALS AND METHODS

Four Bakken Shale samples with varying thermal maturities and organic content were selected for analysis. The RockEval and LECO TOC techniques were used for measuring geochemical properties and organic content of the samples accordingly. One immature sample was selected from the onset of oil generation, namely, BK001; two mature samples from the peak of oil generation, namely, BK002 and BK003; and one overmature sample from the gas window, namely, BK004. The hydrogen index ([HI] a measure of maturity) of these samples ranges from >600 to 6 mg HC/g TOC. Total organic contents (TOCs) range from 21.7 to 7.9 wt%.

Cubical aliquots of approximately 1 cm^3 were collected from each sample, and an 80 μm wide area was polished at the edge of each aliquot using a focused ion beam. The mechanical mapping was conducted using a Hysitron TI950 nanoindenter (Hysitron Inc., Minneapolis, MN, USA) equipped with nano-DMA III.

In composite materials with components of high mechanical contrast, the displacement response of the nano-DMA tip varies depending on the stiffness of the probed grains. A quasi-static load of 2 μN and a dynamic load of 1 μN at a frequency of 200 Hz were maintained on a diamond tip with an 80 nm tip radius while scanning. The applied quasi-static and dynamic load amplitudes on the tip are selected such that its displacement amplitude remains reasonably above the noise floor (0.3 nm for this machine) throughout probing of the surface. Based on the expected range of the elastic modulus of probed grains, from 10 GPa for kerogen as the most compliant grains to 306 GPa for pyrite as the stiffest grains, the contact radius of the used tip may vary between 5.8 and 18.2 nm, respectively (Wilkinson et al., 2014).

The nano-DMA analysis was performed on three 5 μm × 5 μm areas from the polished edge of each aliquot. The modulus maps were analyzed and filtered to remove measurements that were affected by polishing artifacts using the algorithms suggested by Wilkinson et al. (2014). This algorithm detects and masks the neighbor pixels that have a topography difference of greater than 0.3 nm. The filtered areas are excluded from analysis and appear white in the subsequent figures.

Because kerogen-hosted pores have been reported (Slatt and O'Brien, 2011; Loucks et al., 2012; Milliken et al., 2012; Modica and Lapierre, 2012), the samples were investigated for the presence of kerogen-hosted porosity by removing soluble hydrocarbons using solvent extraction followed by subcritical nitrogen adsorption pore size distribution (PSD) and specific surface area (SSA) determination. Solvent extraction was performed on the samples from the oil window to remove the bitumen and liquid hydrocarbon from the pore space. Porosity measured with nitrogen adsorption was found to increase after solvent extraction compared with before extraction.

The measured SSA and PSD curves from subcritical nitrogen adsorption tests are used to characterize the pore system and to determine abundance of kerogen-hosted porosity in each sample.

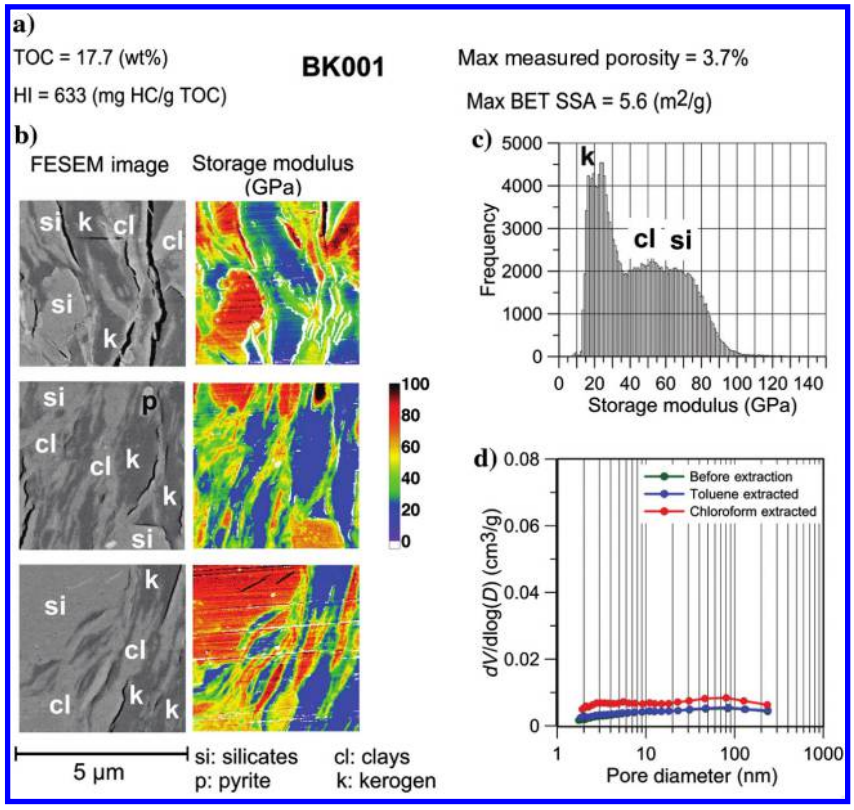

Figure 1. BK001. (a) Geochemical properties and pore characteristics, (b) nanomechanical maps from the surface of the immature sample BK001 and the corresponding FESEM images, (c) histogram of the overall measured elastic modulus values at three areas, and (d) the PSD before and after solvent extraction using toluene and then with chloroform. The lowest measured values correspond to the kerogen particle modulus ranging between 15 and 20 GPa. It is worthwhile mentioning that the desication cracks observed in FESEM images have occurred after nano-DMA tests were performed and have not affected the modulus measurements.

The screened measured values (pixel values that passed the filtering criteria) from all three scans of each sample were analyzed collectively to extract the elastic modulus of the kerogen particle and inorganic minerals. The PSD and SSA were integrated with elastic modulus maps to explain the effect of kerogen-hosted porosity on mechanical modification of the kerogen particles.

RESULTS AND DISCUSSION

The results of modulus mapping, field emission scanning electron microscope (FESEM) images of corresponding mapped areas, geochemical characteristics of the specimen, and PSD curves before and after solvent extraction are shown in the following figures. The histograms show frequency of the collected elastic modulus values in all three scans from each sample (after filtering). In addition to mechanical contrast between the grains, the high resolution of the modulus maps reflect as many textural details as are observed in SEM images.

Sample BK001 is the most immature sample in our selection with an HI of 633 mg HC/g TOC and T_{max} of 428°C. The TOC in this sample is 17.7 wt%.

The histogram of the elastic modulus exhibits a distinct peak in the low range between 15 and 20 GPa. We interpret these low values (15–20 GPa) as reflecting the elastic modulus of larger kerogen particles, and the adjacent peak (approximately 23 GPa) to correspond to thin layers of kerogen, in which the measurements could be affected by the surrounding grains. Moreover, multiple overlapping peaks exist between 40 and 80 GPa, which correspond to clay minerals and quartz particles (Figure 1).

From nitrogen adsorption analysis, this sample shows a very low SSA (maximum of 7.29 m^2/g) and pore volume (maximum of 0.016 m^3/g) before and after solvent extraction. The PSD curve shows a broad distribution of pore sizes throughout the measured interval.

Samples BK002 and BK003 are selected from higher maturity levels at the peak of oil generation. Sample BK002 has an HI of 257 mg HC/g TOC, T_{max} of 442°C, and TOC of 21.7 wt%. Sample BK003 has an HI of 126 mg HC/g TOC, T_{max} of 457°C, and TOC of 7.9 wt%. The elastic modulus histogram of the sample BK002 shows a sharp peak between 7 and 10 GPa (interpreted as the kerogen particle modulus) and overlapping peaks in the range of 15–70 GPa (Figure 2). The modulus histogram of the sample BK003 also shows a copious population of low modulus values between 7 and 10 GPa (kerogen particles). BK003 has a more distinct bimodal distribution between 15 and 70 GPa with peaks at approximately 20 and 60 GPa followed by a very low amplitude broad peak between 100 and 150 GPa representing the modulus of the pyrite grain present in the second scan (Figure 3).

Solvent extraction of these samples resulted in significant increase in SSA (53 and 30 m^2/g), and the PSD curves also exhibited a dramatic change in shape, showing substantial increase in population of nanopores (2–20 nm in diameter), which are indicators of an abundant presence of kerogen-hosted porosity in both samples (Kuila et al., 2014; Zargari et al., 2015).

The two samples show different textural characteristics owing to the high contrast in TOC (21.7 versus 7.9 wt%). The SEM images of sample BK002 show laminated features associated with organo-clay mixtures. These thinly interstratified laminates are also reflected in corresponding modulus maps. However, the fine nature of these features cause interference of measured values, resulting in comingled property measurement in thinly interstratified particles.

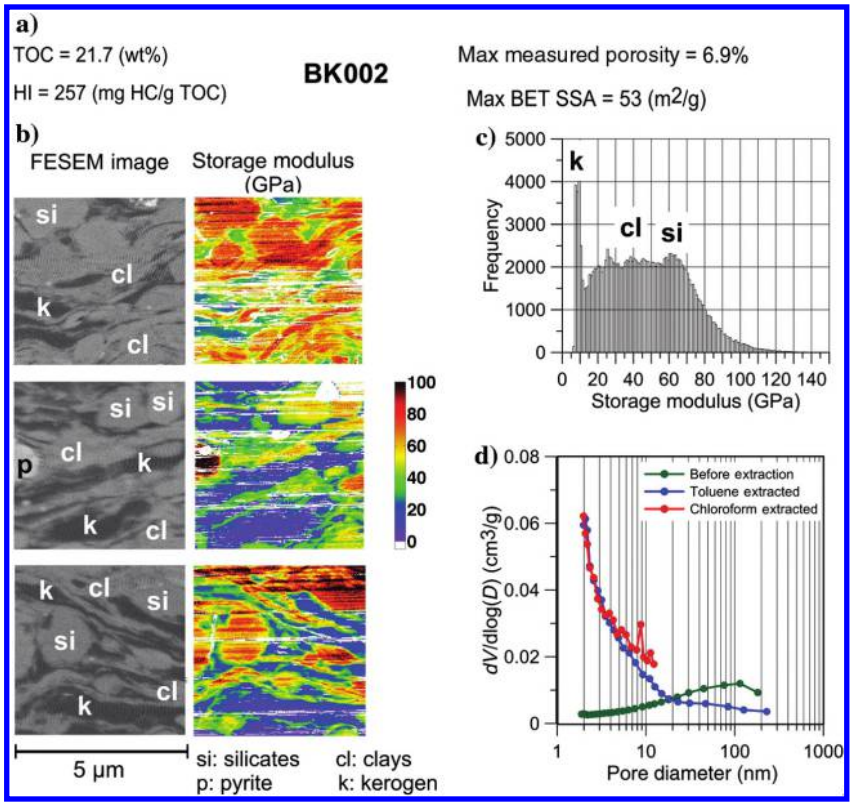

Figure 2. BK002. (a) Geochemical properties and pore characteristics, (b) nanomechanical modulus maps and the corresponding FESEM images, (c) histogram of the measured modulus values, and (d) PSD before and after solvent extraction. Kerogen particles in this sample have an elastic modulus between 7 and 10 GPa.

This effect might compromise a major portion of the measured values in the sample BK002, causing the appearance of the broad peak in the range of 15–70 GPa.

Sample BK004 is the most mature sample in our inventory with an HI of 6 mg HC/g TOC belonging to the overmature gas window, and the TOC is 12.5 wt%. The nitrogen adsorption PSD shows an

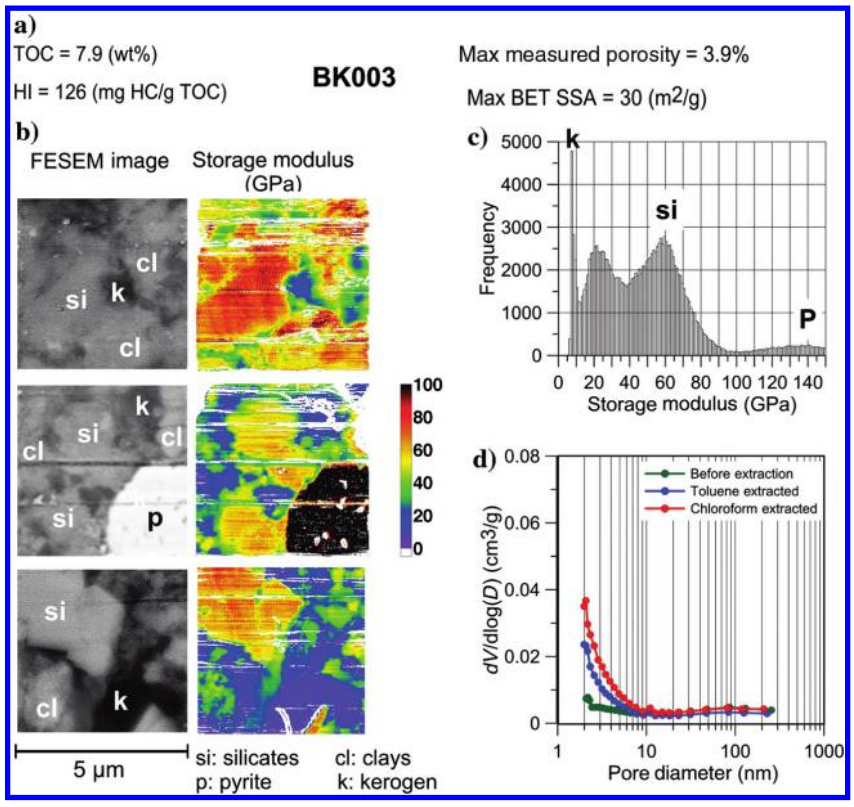

Figure 3. BK003. (a) Geochemical properties and pore characteristics, (b) nanomechanical modulus maps and the corresponding FESEM images, (c) histogram of the measured modulus values, and (d) PSD before and after solvent extraction. Kerogen particles in this sample have an elastic modulus between 7 and 10 GPa.

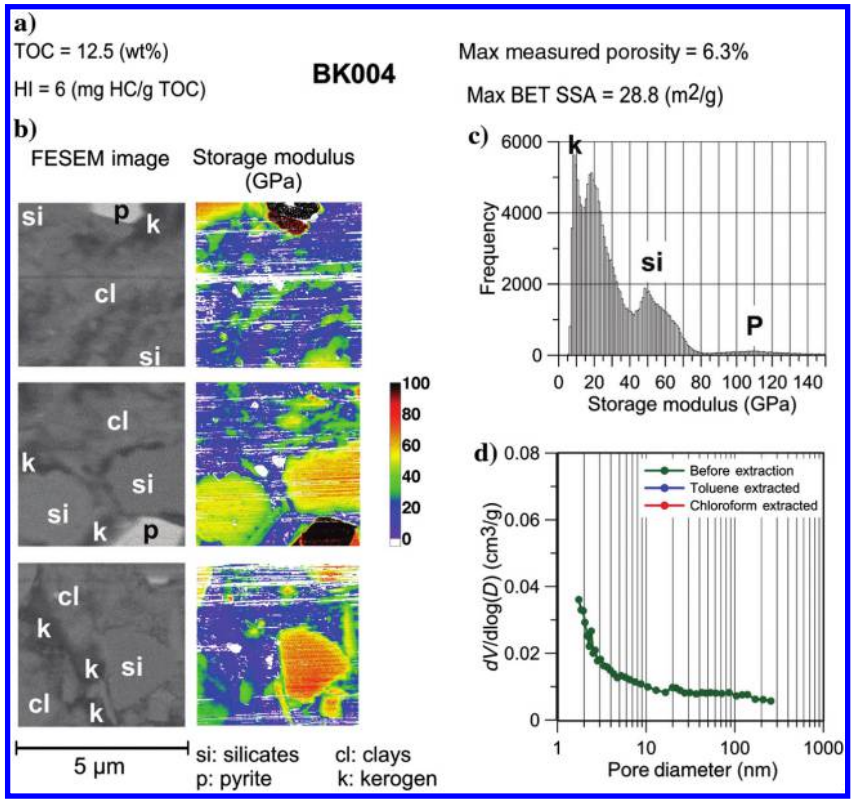

Figure 4. BK004. (a) Geochemical properties and pore characteristics, (b) nanomechanical modulus maps and the corresponding FESEM images, (c) histogram of the measured modulus values, and (d) PSD before and after solvent extraction. Kerogen particles in this sample have an elastic modulus between 7 and 12 GPa.

Table 1. Variations of kerogen particle elastic modulus with maturity as measured using the nano-DMA technique.

Sample	Level of thermal maturity	Kerogen particle modulus (GPa)
BK001	Onset of oil generation (immature)	15–20
BK002	Peak of oil generation (mature)	7–10
BK003	Peak of oil generation (mature)	7–10
BK004	Gas window (overmature)	7–12

abundant presence of nanopores, indicating porosity in the kerogen. The kerogen particle modulus ranges between 7 and 12 GPa. We also observe a second peak between 15 and 30 GPa, which corresponds to thin layers and small pockets of kerogen. The larger kerogen values (second peak) are affected by the underlying and surrounding minerals. The clay minerals and the silicates range in modulus between 45 and 70 GPa represented by the third peak in the histogram (Figure 4).

Here, we find a considerable presence of kerogen-hosted porosity at high maturities. The intraparticle porosity in the kerogen causes a reduction of the elastic modulus of kerogen particles, regardless of whether they are fluid- or gas-filled. These measurements provide us with a good approximation of the kerogen particle modulus that is applicable for rock modeling purposes. These modulus values correspond to the kerogen grains that also contain porosity (Table 1). The kerogen porosity may be filled with water, bitumen, oil, or gas depending on the level of maturity.

These findings are consistent with our previous results in which we studied samples of different maturity at natural and synthetically matured states (Zargari et al., 2013). We observed that the softer portion of the rock, which is comprised of kerogen, clays, and bitumen, is undergoing modulus reduction with natural and synthetic maturity. We previously speculated that the porosity is increasing in the kerogen, causing this modulus reduction, but we were not able to visualize this phenomenon because most of the porosity was filled by the produced hydrocarbons and bitumen.

CONCLUSIONS

A dynamic mechanical analysis (DMA) was performed on four organic-rich shales with thermal maturities ranging from immature to gas window. The nitrogen adsorption pore characterization technique was performed on the samples in their original states and after solvent extraction with toluene and then chloroform to examine the state of the kerogen-hosted porosity.

The immature sample contained minimum kerogen-hosted porosity as indicated by subcritical nitrogen adsorption and exhibited maximum kerogen particle modulus (15–20 GPa).

At higher maturity levels (peak of oil generation and gas window), kerogen particles are more porous, exhibiting extractable hydrocarbons, high SSA, and abundant nanoporosity that lead to lower kerogen particle moduli (7–12 GPa).

By integrating the nanoscale pore characterization and DMA, we showed the significant influence of the intraparticle kerogen porosity on the modulus of kerogen particles.

Determining the solid kerogen modulus, using the results of this study, requires further analysis to collect the information essential for deconvolving the effect of intraparticle kerogen porosity from the kerogen particle properties.

Differentiating between the nanometer/subnanometer pores and solid kerogen to investigate the solid kerogen moduli requires higher resolution measurements or use of deconvolution techniques. To determine the solid kerogen moduli using the results of the current study, we need knowledge of the fraction of porosity in the kerogen, the properties of the pore-filling fluid, and an appropriate model to perform reverse fluid substitution. Further analyses are required to determine these properties.

ACKNOWLEDGMENTS

The data for this paper are available at the Colorado School of Mines data repository. We would like to thank the members of the OCLASSH Consortium at the Colorado School of Mines for financially supporting this project. Special thanks go to L. Canter and the geoscience team at Whiting Petroleum: M. Guisinger, K. Jones, and C. Bugge; and J. Chandler from the SEM laboratory at the Colorado School of Mines for their help with sample preparation.

REFERENCES

Ahmadov, R., T. Vanorio, and G. Mavko, 2009, Confocal laser scanning and atomic-force microscopy in estimation of elastic properties of the organic-rich Bazhenov Formation: The Leading Edge, **28**, 18–23, doi: 10.1190/1.3064141.

Bobko, C., and F. J. Ulm, 2008, The nano-mechanical morphology of shale: Mechanics of Materials, **40**, 318–337, doi: 10.1016/j.mechmat.2007.09.006.

Constantinides, G., K. S. Ravi Chandran, F. J. Ulm, and K. J. Van Vliet, 2006, Grid indentation analysis of composite microstructure and mechanics: Principles and validation: Materials Science and Engineering: A, **430**, 189–202, doi: 10.1016/j.msea.2006.05.125.

Eliyahu, M., S. Emmanuel, R. J. Day-Stirrat, and C. I. Macaulay, 2015, Mechanical properties of organic matter in shales mapped at the nanometer scale: Marine and Petroleum Geology, **59**, 294–304, doi: 10.1016/j.marpetgeo.2014.09.007.

Kuila, U., D. K. McCarty, A. Derkowski, T. B. Fischer, T. Topór, and M. Prasad, 2014, Nano-scale texture and porosity of organic matter and clay minerals in organic-rich mudrocks: Fuel, **135**, 359–373, doi: 10.1016/j.fuel.2014.06.036.

Kumar, V., C. H. Sondergeld, and C. S. Rai, 2012, Nano to macro mechanical characterization of shale: Presented at the SPE Annual Technical Conference and Exhibition.

Loucks, R. G., R. M. Reed, S. C. Ruppel, and U. Hammes, 2012, Spectrum of pore types and networks in mudrocks and a descriptive classification for matrix-related mudrock pores: AAPG Bulletin, **96**, 1071–1098, doi: 10.1306/08171111061.

Mba, K., and M. Prasad, 2010, Mineralogy and its contribution to anisotropy and kerogen stiffness variations with maturity in the Bakken shales: 80th Annual International Meeting, SEG, Expanded Abstracts.

Milliken, K. L., W. L. Esch, R. M. Reed, and T. Zhang, 2012, Grain assemblages and strong diagenetic overprinting in siliceous mudrocks, Barnett Shale (Mississippian), Fort Worth Basin, Texas: AAPG Bulletin, **96**, 1553–1578, doi: 10.1306/12011111129.

Modica, C. J., and S. G. Lapierre, 2012, Estimation of kerogen porosity in source rocks as a function of thermal transformation: Example from the Mowry Shale in the Powder River Basin of Wyoming: AAPG Bulletin, **96**, 87–108, doi: 10.1306/04111110201.

Prasad, M., 2001, Mapping impedance microstructures in rocks with acoustic microscopy: The Leading Edge, **20**, 172–179, doi: 10.1190/1.1438902.

Prasad, M., M. Kopycinska, U. Rabe, and W. Arnold, 2002, Measurement of Young's modulus of clay minerals using atomic force acoustic microscopy: Geophysical Research Letters, **29**, 13-1–13-4, doi: 10.1029/2001GL014054.

Prasad, M., K. C. Mba, T. Sadler, and M. L. Batzle, 2011, Maturity and impedance analysis of organic-rich shales: SPE Reservoir Evaluation and Engineering, **14**, 533–543, doi: 10.2118/123531-PA.

Shukla, P., 2013, Nanoindentation studies on shales: Ph.D. thesis, Mewbourne School of Petroleum and Geological Engineering, University of Oklahoma.

Slatt, R. M., and N. R. O'Brien, 2011, Pore types in the Barnett and Woodford gas shales: Contribution to understanding gas storage and migration pathways in fine-grained rocks: AAPG Bulletin, **95**, 2017–2030, doi: 10.1306/03301110145.

Ulm, F. J., and Y. Abousleiman, 2006, The nanogranular nature of shale: Acta Geotechnica, **1**, 77–88, doi: 10.1007/s11440-006-0009-5.

Ulm, F. J., M. Vandamme, H. M. Jennings, J. Vanzo, M. Bentivegna, K. J. Krakowiak, G. Constantinides, C. P. Bobko, and K. J. Van Vliet, 2010, Does microstructure matter for statistical nanoindentation techniques?: Cement and Concrete Composites, **32**, 92–99, doi: 10.1016/j.cemconcomp.2009.08.007.

Vernik, L., and A. Nur, 1992, Ultrasonic velocity and anisotropy of hydrocarbon source rocks: Geophysics, **57**, 727–735, doi: 10.1190/1.1443286.

Wilkinson, T. M., S. Zargari, M. Prasad, and C. E. Packard, 2014, Optimizing nano-dynamic mechanical analysis for high-resolution, elastic modulus mapping in organic-rich shales: Journal of Materials Science, **50**, 1041–1049, doi: 10.1007/s10853-014-8682-5.

Zargari, S., K. L. Canter, and M. Prasad, 2015, Porosity evolution in oil-prone source rocks: Fuel, **153**, 110–117, doi: 10.1016/j.fuel.2015.02.072.

Zargari, S., M. Prasad, K. C. Mba, and E. D. Mattson, 2013, Organic maturity, elastic properties, and textural characteristics of self resourcing reservoirs: Geophysics, **78**, no. 4, D223–D235, doi: 10.1190/geo2012-0431.1.

Zeszotarski, J. C., R. R. Chromik, R. P. Vinci, M. C. Messmer, R. Michels, and J. W. Larsen, 2004, Imaging and mechanical property measurements of kerogen via nanoindentation: Geochimica et Cosmochimica Acta, **68**, 4113–4119, doi: 10.1016/j.gca.2003.11.031.